Journal of Industrial Technology 12 (2), 2003, 23-36

ANALYSIS OF LEAD COUNT EFFECT ON GAP FORMATION IN THE SEAL USED FOR LEAD FRAME ELECTROPLATING PROCESS

Zaidi Mohd Ripin, Tee Boon Hoo and Ahmad Baharuddin Abdullah
School of Mechanical Engineering
Universiti Sains Malaysia, Engineering Campus
14300 Nibong Tebal, Penang, Malaysia.
(mezaidi@eng.usm.my)

***RINGKASAN**: Bingkai pendulu biasanya di rekabentuk dan dihasilkan untuk membentuk jaringan asas logam bagi litar bersepadu. Saiz dan geometri titik tersadur yang dikehendaki akan disadurkan pada bingkai pendulu melalui proses elektropenyaduran. Kedap berfungsi menentukan geometri kawasan yang perlu disadur dengan menghadkan aliran elektrolit di dalam kawasan saduran sahaja. Kedap terdiri daripada dua bahagian, kedap bahagian atas diperbuat daripada elastomer berasaskan silikon manakala kedap yang dibawah diperbuat daripada lapisan nipis elastomer pada bahan seakan-akan span. Kebocoran akan berlaku pada keadaan tertentu, yang mana akan menyebabkan produk tidak diterima. Ini disebabkan celah yang terhasil di antara pendulu dan kedap. Celah yang terhasil pada keadaan operasi sebenar akan membenarkan elektrolit mengalir keluar dan menyadurkan logam di bahagian luar daripada geometri yang dikehendaki. Malah adalah penting untuk memahami pembentukan celah untuk mengawal sepenuhnya proses penyaduran ini. Salah satu daripada paramater yang mempengaruhi pembentukan celah ialah bilangan pendulu pada bingkai pendulu. Model dua dimensi analisis unsur terhingga telah dijalankan dengan menggunakan model bahan Mooney-Rivlin untuk elastomer dan model bahan Blatz-Ko untuk bahan berspan. Analisis sentuhan digunakan untuk menentukan kawasan sentuhan, dan kawasan tidak sentuh akan diketahui daripada celah antara pendulu dan kedap. Beberapa tingkat beban digunakan di dalam analisis untuk memerhatikan pengurangan saiz celah pada beban yang dikenakan. Keputusan telah menunjukkan yang luas celah menjadi semakin mengecil apabila beban dikenakan, dengan kecenderungan untuk mengurang dengan lebih cepat untuk bilangan celah yang lebih rendah. Saiz celah maksimum secara konsisten terhasil pada lokasi celah pertama dan terakhir. Saiz celah yang maksimum akan digunakan sebagai pengukur prestasi kedap dan apabila diplotkan melawan tingkat beban telah menunjukkan pengurangan luas celah apabila beban meningkat. Keputusan-keputusan ini membuktikan bahawa bilangan pendulu adalah parameter penting yang mempengaruhi luas celah.*

ABSTRACT: Lead frame is intricately designed and engineered to form the basic metal base network of an integrated circuit. Desired geometry and size of plated spots are deposited onto the lead frame through the electroplating process. An intermittent seal carries out the task of defining the plated geometry by limiting the flow of electrolyte within the plated area. The seal is made of two parts, the top seal is made from silicone base elastomer while the bottom seal is made from a layer of thin elastomer on a sponge-like material. Leakage that causes product reject still occurs under certain conditions. This is believed to be caused by the gap existing between the lead and the seal. The gap that exists under actual operating condition will allow the electrolyte to seep through and deposit excess metal outside the specified geometry. Thus, it is important to understand the formation of gaps to fully control the plating process. One of the parameters which influence the gap formation is the lead count on the lead frame. A two-dimensional finite element analysis was carried out using Mooney-Rivlin material model for the elastomer and Blatz-Ko material model for the sponge material. The contact analysis is used to determine areas of contact with the non-contact area identified as the gap between the lead and the seal. Several load steps were used in the analysis to monitor the gap size reduction with the applied load. Different numbers of leads were used in the analysis to determine the effect of lead count on the gap formation. The results showed that gap area becomes smaller as the applied load increase, with the tendency to decrease more rapidly for the lower lead count. The maximum gap size consistently occurs at the first and last inner gap. The maximum gap size was used as the performance measure of the seal and when plotted against the load step showed a trend of decreasing gap area as the load increase. The results indicated that lead count is an important parameter affecting the gap area.

KEYWORDS: Electroplating, intermittent seal, finite element method, gap

INTRODUCTION

Lead frame manufacturing is one of the important industries supporting the integrated circuit manufacturing sector in Malaysia (Dynacraft). To increase competitiveness, defects on lead frame manufacturing must be removed or reduced in order to increase productivity. The lead frame manufacturing technology that also entails the electroplating process, is still needed to service the requirement of the lower end of packaging which is currently facing stiff competition from other competing technologies particularly Ball Grid Array (BGA) and more recently Chip Scale Package (CSP). Chip to package connection design particularly Dual In Line Package (DIP) and Quad Flat Package (QFP) with lower input/output of about 500 are still viable for lower performance chips (Tummala, 2001). However since lead frame is an established technology it is still competitive to be produced in Malaysia. Figure 1 shows a typical copper lead frame with 64 leads. The centre window is the area where a silver layer is electroplated on the copper surface. The electrolyte used is aqueous solution of argentum cyanide. To limit and control the geometry of the electroplated area, a rubber mask is used. The rubber mask is made from silicon-based elastomer to withstand the temperature and corrosive nature of the electrolytes. The design of the mask is based on the face seal concept where the overall area is sealed and only the desired area to be electroplated is exposed. This is different from the more widely used and analysed O-ring seals where sealing occurs under relatively high pressure in order to force rubber deformation to close any gaps at the mating surfaces (Greene, 1997). This paper describes the analysis undertaken to understand the gap formation at the seal used in lead frame electroplating process.

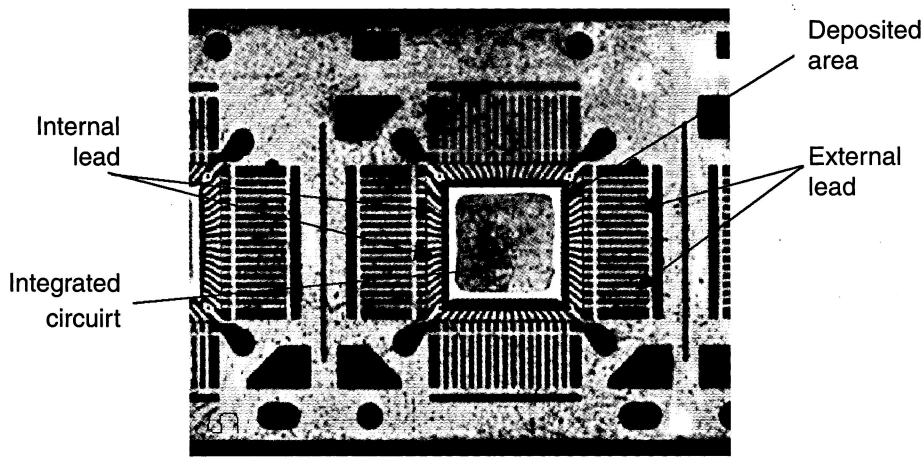

Figure 1. *Lead frame with 64 leads*

One of the important and basic components of an integrated circuit is the lead frame, which acts as the basic metal base network. Electroplating is one of the core processes in the manufacturing of lead frame. This process deposits the desired geometry and size of the plated spots on the lead frame. The accuracy of the electroplated spot or area depends greatly on the performance of the electroplating seal, which is an intermittent type seal. In general there are two types of seal. The first is the static seal where the mating surfaces do not move relative to each other, typical example is the gasket. The second is the dynamic seal where the mating surfaces move relative to each other, the mechanical seal is a typical example. In the electroplating process, the seal is active (i.e. the mating surface comes together) for the duration of the electroplating process which is about 90 seconds. The seal is separated into two halves to allow the plated lead frame to move forward and replaced by next lead frame. The process is intermittent. An ideal seal will cover the lead frame, allowing only the exposed surface to be electroplated. In actual case, under certain operating conditions, a gap is formed between the lead and the seal that will allow the electrolyte to seep through, thus depositing excess metal outside the boundary. This gap formation depends on the lead counts and the overall geometry of the lead frame. As pressure is applied on the seal to close the gap, the dimension and overall geometry of the seal changes, thus changing the geometry of the exposed area and making it more difficult to control the dimensions and geometry of the electroplated spots on the lead frame. Therefore the geometry of the seal, lead frame and the pressure pad affect the performance of the seal. Seal material, usually elastomeric, with its non-linear, hyperelastic and incompressible characteristic, makes it difficult to control this process (Allport & Day, 1996). A precisely designed seal will allow compensation on the geometry changes and minimise gap formation. Elastomer seal designs are commonly developed on the basis of prior experience, part prototyping, and extensive experimental testing (Gregory *et al.*, 1997). This paper describes the analysis of the intermittent seal using the finite element method in order to understand gap formation of the seal under operating condition. Contact elements are used to determine the interface contact area, the associated stress distribution within the rubber seal and in particular, the gap geometry. Evaluation on the effects of lead counts on the lead frame in relation to gap formation is carried out.

METHOD

In order to reduce the computational time required for the analysis to a reasonable level, the analysis is carried out using a two-dimensional model. A number of models will be constructed with different number of lead counts. A general model used for the analysis is shown in Figure 2. A number of leads are placed between the face seal and the pressure pad. For this paper, the analysis will be carried out on models with lead counts of 4 to 10. The lead frame design shown in Figure 1 has 16 leads at each side. Figure 2 clearly shows that gaps exist at the face seal and the pressure pad at the initial state. The gaps are numbered as shown in Figure 3.

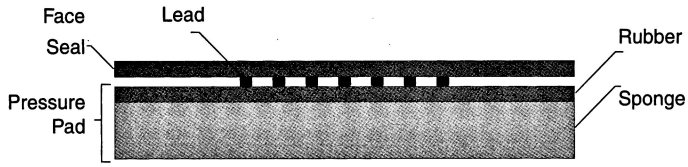

Figure 2. *A general model for the analysis*

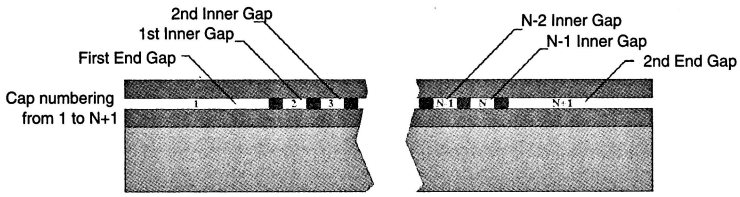

Figure 3. *Numbering of the gaps*

Both elements in contact with the leads are made from elastomeric material in the actual electroplating process. The face seal is made from a single layer of silicone rubber whereas the pressure pad is constructed with a layer of silicone rubber on top and sponge at its bottom portion. Even though the Arruda-Boyce material model is better, its application is provided only for three-dimensional analysis in the software used (Ansys, 2000). The Mooney-Rivlin material model is used in this two-dimensional analysis and will be described in detail later in the paper. The rubber or elastomeric component is meshed with a 4-node hyperelastic element with Mooney-Rivlin constitutive model properties, and the sponge component is meshed with a 4-node Blatz-Ko hyperelastic element (Kohnke, 1999). The areas or regions of contact or potential to come in contact are meshed with two-dimensional surface to surface contact element. A compromise had to be made on the element size as finer element size will mean longer computational processing time (Keene & Prior, 1997). Figure 4 shows the meshed model. An increasing top pressure that simulates the operating pressure in the actual plating process was applied onto the top surface of the face seal. The pressure was applied gradually in 8 load steps with the final pressure of 0.135 MPa to represent the actual pressure during operation. The model was then analysed and the results discussed.

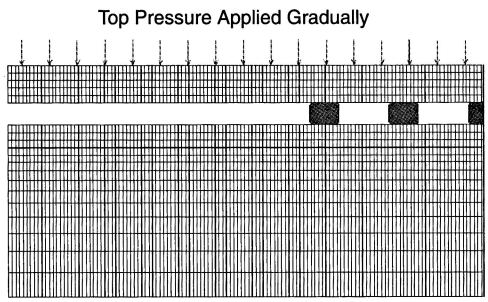

Figure 4. *Meshed model with load applied*

MATERIAL MODEL

The Mooney-Rivlin model relates the strain energy, W to the principle stretch, λ_1, λ_2 and λ_3 (Allport & Day, 1996)

$$W = C_1(\lambda_1^2+\lambda_2^2+\lambda_3^2-3)+C_2\left(\frac{1}{\lambda_1^2}+\frac{1}{\lambda_2^2}+\frac{1}{\lambda_3^2}-3\right)$$

$$\text{where } \lambda = \frac{\text{Final Length}}{\text{Initial Length}}$$

The constants C_1 and C_2 for the equation above can be obtained from experimental data.

The Arruda-Boyce model gives the stress-stretch relationship as follows;

$$\sigma_1-\sigma_2 = \frac{nk\Theta}{3}\sqrt{N}L^{-1}\left(\frac{\lambda_{chain}}{\sqrt{N}}\right)\left[\frac{\lambda^2_1-\lambda^2_2}{\lambda_{chain}}\right]$$

where,

$\frac{nk\Theta}{3} = C_R$ = Rubber Modulus
n = Chain density
k = Boltzmann constant
Θ = Absolute temperature
$L^{-1}(\beta)$ = Langevin Inverse Function

$$= 3\beta+\frac{9}{5}\beta^3+\frac{297}{175}\beta^5+\frac{1539}{875}\beta^7+\frac{126117}{67375}\beta^9+.....$$

$$\lambda_{chain} = \frac{r_{chain}}{r_o}$$

$$= \frac{1}{\sqrt{3}}(\lambda_1^2+\lambda_2^2+\lambda_3^2)^{1/2}$$

This model was proven accurate when compared to the earlier experiment by Treloar (1946). As the Arruda-Boyce model is not supported in the software used for two-dimensional analysis, the Mooney-Rivlin material model had to be adopted. In order to find the best material model, the parameters for the Arruda-Boyce model were determined first since the parameters are not dependent on the types of loading and deformation (Arruda & Boyce, 1993; Akron & Arruda, 1998; Allport & Day, 1996; Kohnke, 1999). In this work a uniaxial compression test was carried out on the seal sample (dimethyl silicone rubber). This experiment is necessary to determine the parameters for the Arruda-Boyce model.

Experimental Set-up

The plain strain compression test was carried out based on Arruda & Boyce (1993) and Bergstrom (1999). The specimen of size 12x9x12 mm was located within a confined space where the 9mm dimension was constrained. The specimen was well-lubricated using lubricating oil to minimise friction. The axial load was applied gradually using hydraulic cylinders at the speed of 0.1 mm/s. The displacement was measured using an indicator and the force was measured with a load cell (Kyowa, 50 kgf, type L).

Results

The resulting stretch and stress was fed into a programme (MathCAD 2000) using non-linear regression to obtain the required parameter. The required stress-stretch relationship in the MathCAD 2000 form is shown below:

$$F(z,u) := \begin{bmatrix} 3\text{-}u_0\text{-}\left(z\text{-}\frac{1}{z^3}\right)\text{-}\left[1+\left(\frac{1}{5}\right)\text{-}\left[\frac{\left(z^2+\frac{1}{z^2}+1\right)^1}{(u_1)^2}\right]+\left(\frac{11}{175}\right)\text{-}\left[\frac{\left(z^2+\frac{1}{z^2}+1\right)^2}{(u_1)^4}\right]+\left(\frac{19}{875}\right)\text{-}\left[\frac{\left(z^2+\frac{1}{z^2}+1\right)^3}{(u_1)^6}\right]+\left(\frac{519}{67375}\right)\text{-}\left[\frac{\left(z^2+\frac{1}{z^2}+1\right)^4}{(u_1)^8}\right]\right] \\ 3\text{-}\left(z\text{-}\frac{1}{z^3}\right)\text{-}\left[1+\left(\frac{1}{5}\right)\text{-}\left[\frac{\left(z^2+\frac{1}{z^2}+1\right)^1}{(u_1)^2}\right]+\left(\frac{11}{175}\right)\text{-}\left[\frac{\left(z^2+\frac{1}{z^2}+1\right)^2}{(u_1)^4}\right]+\left(\frac{19}{875}\right)\text{-}\left[\frac{\left(z^2+\frac{1}{z^2}+1\right)^3}{(u_1)^6}\right]+\left(\frac{519}{67375}\right)\text{-}\left[\frac{\left(z^2+\frac{1}{z^2}+1\right)^4}{(u_1)^8}\right]\right] \\ \text{-}3\text{-}u_0\text{-}\left(z\text{-}\frac{1}{z^3}\right)\text{-}\left[\left(\frac{2}{5}\right)\cdot\left[\frac{\left(z^2+\frac{1}{z^2}+1\right)^1}{(u_1)^3}\right]+\left(\frac{44}{175}\right)\text{-}\left[\frac{\left(z^2+\frac{1}{z^2}+1\right)^2}{(u_1)^5}\right]+\left(\frac{114}{875}\right)\text{-}\left[\frac{\left(z^2+\frac{1}{z^2}+1\right)^3}{(u_1)^7}\right]+\left(\frac{4152}{67375}\right)\text{-}\left[\frac{\left(z^2+\frac{1}{z^2}+1\right)^4}{(u_1)^9}\right]\right] \end{bmatrix}$$

$F(z, u)$ = Nominal Stress

u = Parameter or Constant

u_o = Rubber Modulus

$$= \frac{nk\Theta}{3}$$

u_1 = λ_L = Stretch Limit

$$= \sqrt{N}$$

z = Stretch

$$= \lambda$$

The Arruda-Boyce parameter obtained are as follows:

Rubber modulus, $\frac{nk\Theta}{3} = C_R = 0.093$ MPa

Stretch limit, $u_1 = \lambda_L = \sqrt{N} = 7.905$

Bulk modulus, B = 50 MPa (approximate value)

The above parameters were used in the finite element analysis of the test specimen to compare the finite element behaviour in order to verify the model.

Figure 5 shows the stress-stretch curves for the experimental, theoretical and FE simulation. The curve compares well for stretch values of 1 to 0.5. After the stretch value of 0.5, the theoretical and experimental data still compared well with difference less than 3%. However the difference for the FE simulation values is quite significant, thus the FE model can only be reliable for stretch values between 1.0 to 0.5. Since the pressure applied on the seal used is less than 1 MPa, the FE model is considered valid for the subsequent analysis. The two-dimensional finite element model was subsequently developed using Mooney-Rivlin material model for two parameters even though the software used could support up to nine parameters. Table 1 shows the material parameters used for the Mooney-Rivlin model.

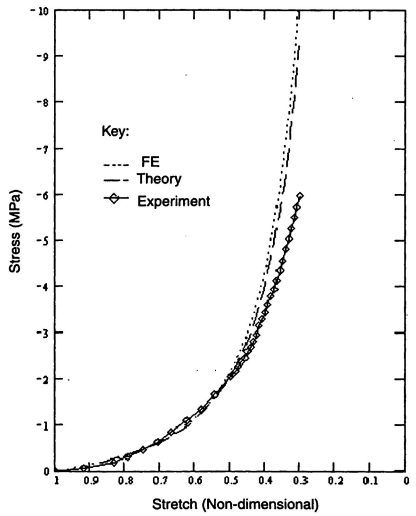

Figure 5. *Comparison of relationship between stress and stretch for experimental, theoretical and FE simulation*

Table 1. Parameters for the Mooney - Rivlin model

Material : dimethyl silicone rubber	
Modulus Young, *E*	2.83 MPa
Poisson Ratio, *v*	0.49
Mooney-Rivlin constant	
C1	0.1915
C2	-0.03043

Figure 6 shows the strain-stress diagram for the finite element model using the 3-D Arruda-Boyce material model and 2-D Mooney-Rivlin material model. The result indicates the Mooney-Rivlin model gives slightly higher values of strain for a given stress compared to the Arruda-Boyce model. The overall difference is less than 2.5%. Therefore the Mooney-Rivlin material model with the associated parameters was adopted in the subsequent 2-D analysis.

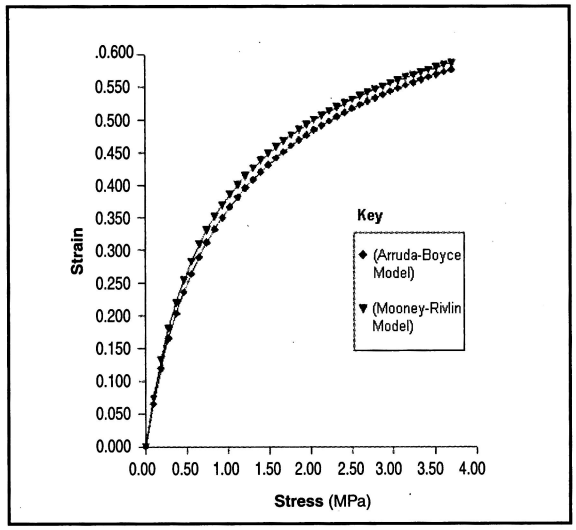

Figure 6. *Strain - stress relationship for specimen model with Arruda-Boyce and Mooney-Rivlin material model*

Sponge

The bottom pressure pad consists of a sponge material overlaid with a 2mm layer of silicon based elastomer. To model the sponge, the material model known as open cell sponge (Kohnke, 1999) was used with Young's Modulus of 1.00 MPa and Poisson ratio of 0.3. Hyper-elastic elements were used to model the sponge.

RESULTS AND DISCUSSION

At the end of the loading process, the face seal and the pressure pad deformed as shown in Figure 7. The face seal was forced to come in contact with the pressure pad thereby reducing the gaps that exist between them. The result in Figure 7 shows there was no gap outside the lead region but gaps exist in the areas between the leads indicating the possible route for electrolyte to seep through. The gaps that exist on a general model is shown in Figure 2. In Figure 8, the gaps are identified by a numbering system that labels the inner gap separately, that is the gap between the first and second leads is taken as the first inner gap. Figure 8 also

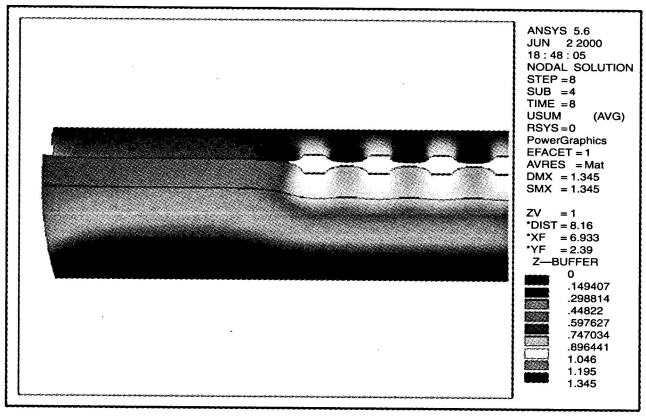

Figure 7. *Final model face seal and pressure pad after load step no. 8*

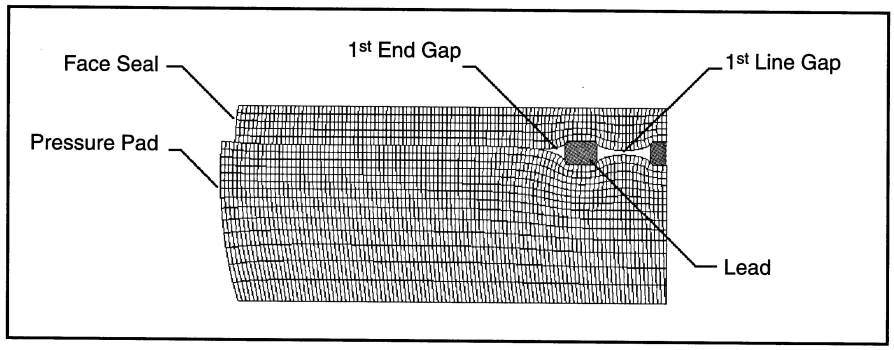

Figure 8. *Gaps between face seal and pressure pad*

shows the gap cannot be closed even after the maximum pressure is applied to the seal. The changes on the gaps as pressure is applied onto the seal will be measured in terms of the gap area. The total gap area is the summation of all the gap areas that exist in the seal. Figure 9 shows the changes in total gap area plotted against load steps for lead counts of 4 to 10. LC_*n* represents *n* number of lead counts. At the initial state (no loading), the total gap area is largest for the model with the lowest lead counts, and reduces as the lead counts increases. From Figure 9, it is clearly seen that the rate of reduction of the total gap area decreases as the number of lead counts increase. In other words, the total gap area decreases more rapidly for a lower number of lead counts model. At the end of the pressure application, the minimum total area occurred for models with lower lead counts, that is lead counts of 4 and 5. This indicates that the effects of small numbers lead counts on gap formation can be neglected. The final total gap area increased with the larger number of lead counts (6 onwards) indicating increased difficulty to close or minimise the gaps between the seal and pressure pad. For the same gap area, a higher pressure had to be applied on models with higher number of lead counts.

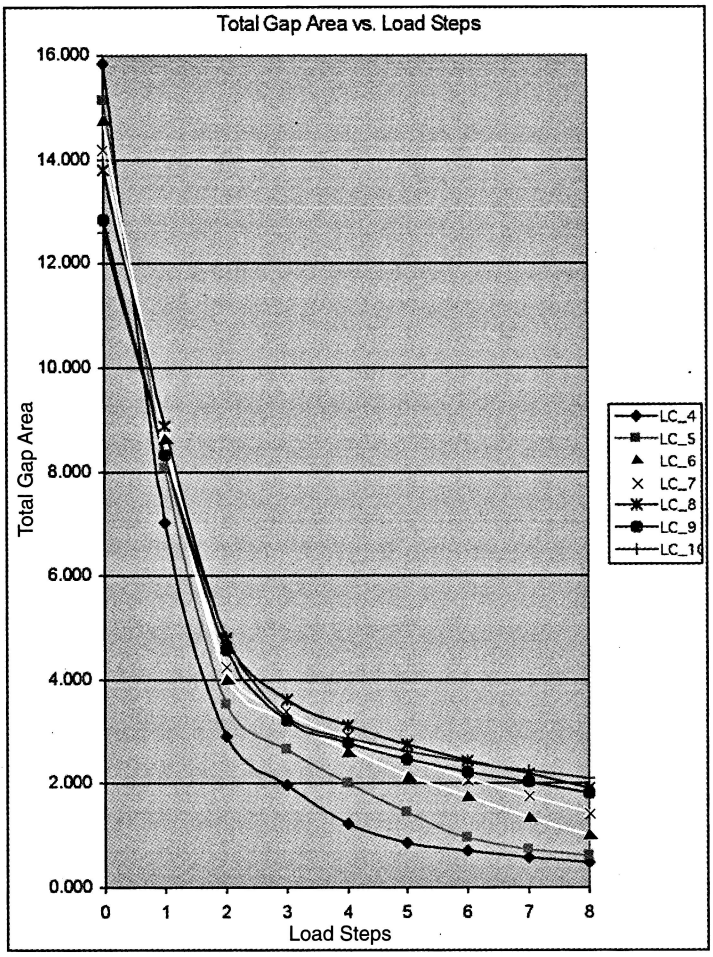

Figure 9. *Changes in the total gap area versus load steps for various number of lead counts (LC=Lead Count)*

Figure 10 shows the distribution of gap area on different gap number for lead counts of 4 to 10. From the graphs, it is clear that the maximum gap area will always occur at the second gap or the first inner gap. This phenomenon can be explained by the seal and pressure pad material being forced to flow outwards and downwards or upwards to close the gap between the leads as the seal is pressed onto the leads. As shown in Figure 7, the seal and pressure pad will swell extensively at the end of the loading process. This showed the material has greater tendency to flow outwards since the stress level is lower at the outer edge. The flow of material towards the edge will reduce the tendency of the material at the inner gaps to flow downwards or upwards. The first and last inner gaps which are closest to the edge will suffer the most, while gaps located toward the middle of the seal or pressure pad experience reduced effect.

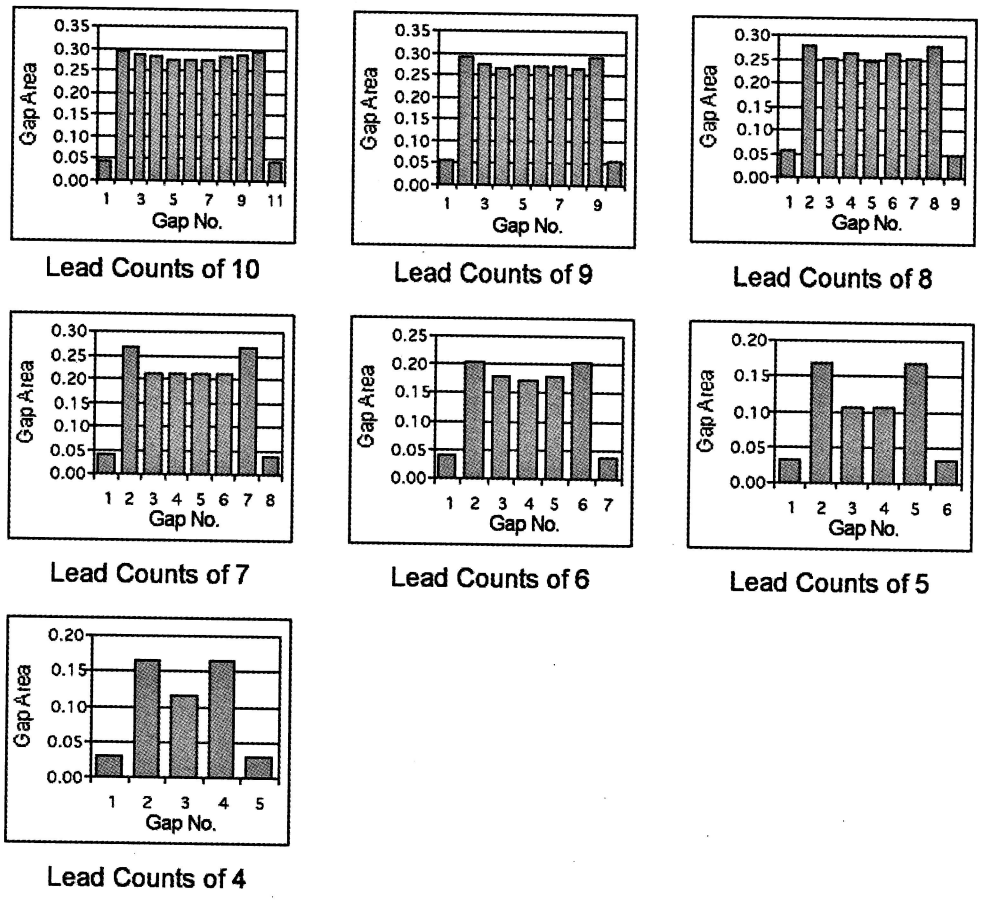

Figure 10. *Distribution of gap area at different gap number*

Another important observation from Figure 10 is the gap area between the leads are not uniform for any given lead count where the distribution of the gap area forms a depression with the minimum gap area in the middle. These two observations explains the tendency of leak to occur at the first inner gaps rather than elsewhere due to their relatively larger size.

The maximum gap size will ultimately determine the performance of the seal as shown in the plot of maximum gap size against load steps in Figure 11. As shown previously, the initial inner gap area reduces as the number of lead counts increases. The changes in the maximum gap area with the load steps exhibit the same behaviour as the total gap area except that the rate of decrease in maximum gap area is smaller. Until load step 3, the models with larger number of lead counts still had the larger maximum gap area. After load step 3, due to higher decreasing rate, the models with lower number of lead counts tend to have smaller maximum gap areas. The changes in the maximum gap area with different lead counts show decreasing

rates, suggesting that a minimum gap amount will always exist. At the end of the analysis, the models with smaller number of lead counts have smaller gap areas compared to models with larger number of lead counts. The larger difference in lead counts resulted in greater difference in the individual gap areas. However as shown in Figures 9 and 11, this statement is only true for models with large number of lead counts. The lead counts effect could be neglected for models with small number of lead counts

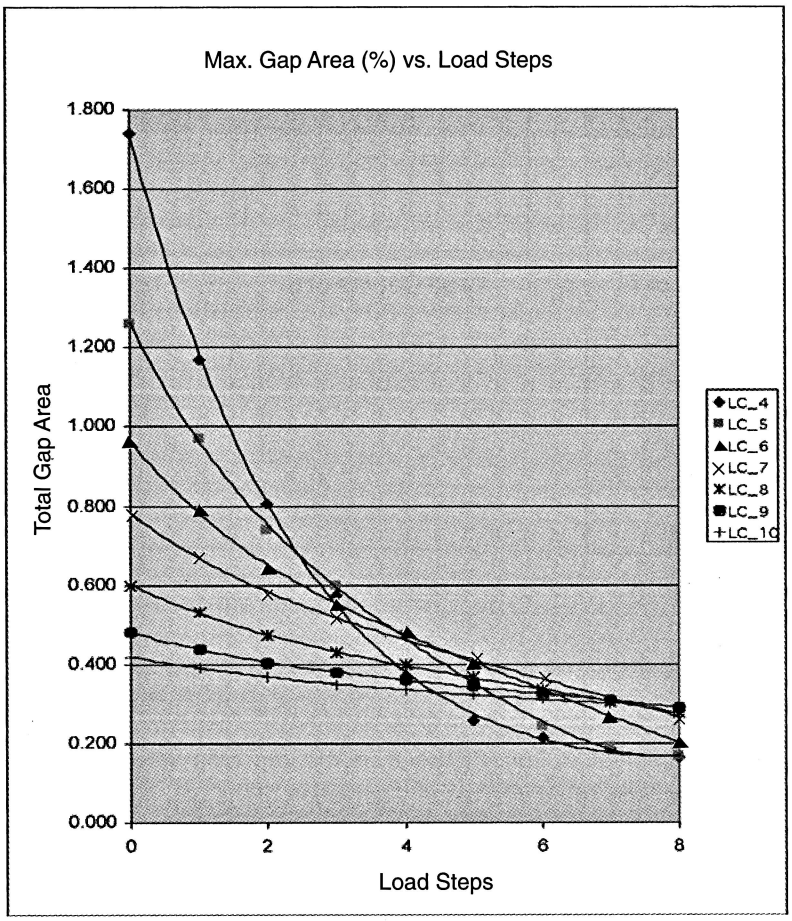

Figure 11. *Maximum gap area versus load steps*

Figure 12 shows the relation of maximum gap area to the load steps. Models with smaller number of lead counts have lower values of gap area at any given load step. This indicates that gaps for lower lead counts models are easily reduced.

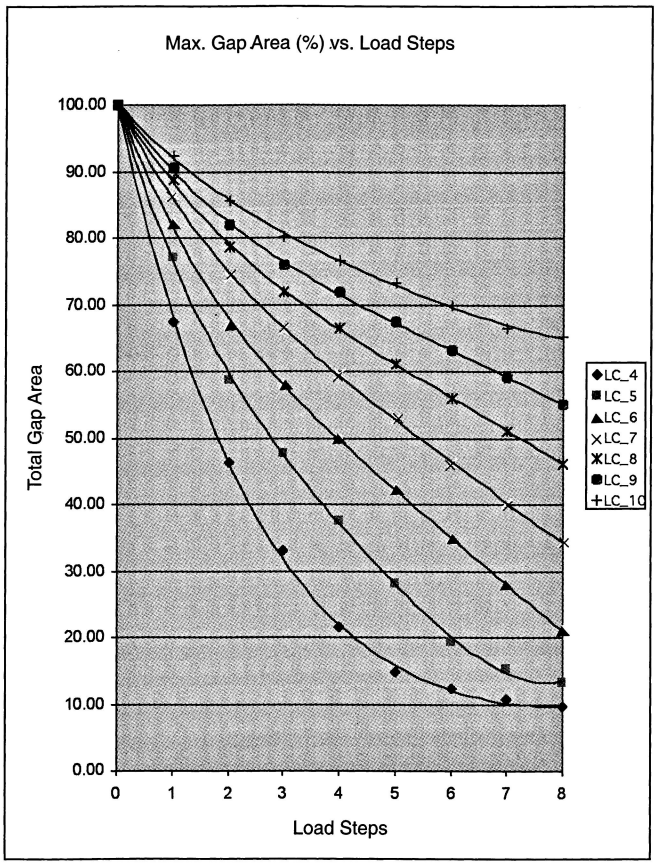

Figure 12. *Maximum gap area (%) versus load steps*

CONCLUSION

A two dimensional finite element method analysis was carried out using the Mooney-Rivlin material model, where the value of stress derived from experimental data is 2.5% higher for a given strain compared to the Arruda-Boyce model.

The contact analysis showed the number of leads affects the gap formation in the seal. At the early stage of pressure loading, models with lower lead counts have bigger total gap areas. As the load increases the total gap area on models with lower lead counts have higher decreasing rate and after the final load step at 0.185 MPa, the lower lead counts models have smaller values of total gap areas.

The maximum gap areas always occur at the first and last inner gaps. These maximum gaps exhibit the same behaviour as the total gap areas.

ACKNOWLEDGEMENT

The authors would like to thank the School of Mechanical Engineering and Universiti Sains Malaysia for their full support and Ministry of Science, Technology and the Environment for their sponsorship of this project through the IRPA grant.

REFERENCE

Akron, P. A. and Arruda, E. M. (1998). Experimental investigation and modeling of incompressible elastomer during non-homogeneous deformation. *Rubber Chem. and Tech.* **71**(4): pp 730.

Ansys, Inc., (2000). *Ansys Solutions.* Canonsburg: Ansys, Inc. **2**(4).

Arruda, E. M. and Boyce, M. C. (1993). A three-dimensional constitutive model for the large stretch behaviour of rubber elastic materials. *J. Mech. Phys. Solids,* **41**(2): pp 389-412.

Allport, J. M. and Day, A. J. (1996). Statistical mechanics material model for the constitutive modelling of elastomeric compounds. *J. of Mech. Engrs. Sci.* Part C: pp 575-585.

Bergström, J. S. (1999). *Large strain time-dependent behaviour of elastomeric materials.* Thesis (PhD). Massachusetts Institute of Technology.

Dynacraft Industries Sdn. Bhd., http://www. dynacraft.com.

Greene, Tweed and Co. (1997). *The right seal: Your guide to sealing in semiconductor processing.* USA: Greene, Tweed & Co.

Gregory, I. H., A. H. Muhr and I. J. Stephens. (1997). Engineering applications of rubber in simple extension. In: *Plastic, rubber and composites processing and applications.* **26**(3): pp 118 - 122.

Keene, R. and Prior, A. (1997). Analysis of axisymmetric elastomeric components subjected to asymmetric loading. In: *Plastic, rubber and composites processing and applications.* **26**(3): pp 123-128.

Kohnke, P. (1999). *ASYSY Theory Reference: Release 5.6.* Southpointe: ANSYS. Inc, pp 4-1 - 4-50.

Treloar, L. R. G. (1946). The elasticity of a network of long chain molecules, Part III. *Trans. Faraday Soc.* **42**: pp 83-94.

Tummala, (2001). *Fundamentals of microsystems packaging*, Mc Graw Hill, New York, pp 68-77.